

Selective Photoinduced Antibacterial Activity of Amoxicillin-Coated Gold Nanoparticles: From One-Step Synthesis to in Vivo Cytocompatibility

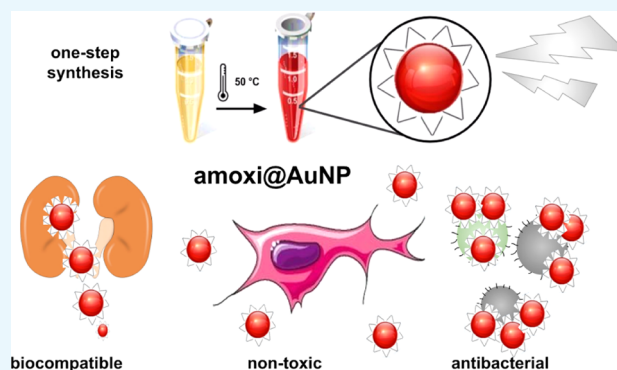
M. Jazmín Silvero C.,^{†,‡} Diamela M. Rocca,[‡] Emilce Artur de la Villarmois,[§] Kelsey Fournier,[†] Anabel E. Lanterna,[†] Mariela F. Pérez,[§] M. Cecilia Becerra,^{*,‡} and Juan C. Scaiano^{*,†}

[†]Department of Chemistry and Biomolecular Sciences and Centre for Advanced Materials Research (CAMaR), University of Ottawa, 10 Marie Curie, Ottawa, Ontario K1N 6N5, Canada

[‡]Instituto Multidisciplinario de Biología Vegetal (IMBIV-CONICET), Departamento de Ciencias Farmacéuticas and [§]Instituto de Farmacología Experimental Córdoba (IFEC-CONICET), Departamento de Farmacología, Facultad de Ciencias Químicas, Universidad Nacional de Córdoba, Haya de la Torre S/N, Córdoba X5000, Argentina

Supporting Information

ABSTRACT: Photoinduced antibacterial gold nanoparticles were developed as an alternative for the treatment of antibiotic-resistant bacteria. Thanks to the amoxicillin coating, they possess high in vivo stability, selectivity for the bacteria wall, a good renal clearance, and are completely nontoxic for eukaryotic cells at the bactericidal concentrations. A simple one-step synthesis of amoxi@AuNP is described at mild temperatures using the antibiotic as both reducing and stabilizing agent. Time-resolved fluorescence microscopy proved these novel nano-photosensitizers, with improved selectivity, are bactericidal but showing excellent biocompatibility toward eukaryotic cells at the same dose (1.5 $\mu\text{g}/\text{mL}$) when co-cultures are analyzed. Their stability in biological media, hemocompatibility, and photo-antibacterial effect against sensitive and antibiotic-resistant *Staphylococcus aureus* were evaluated in vitro, whereas toxicity, renal clearance, and biodistribution were studied in vivo in male Wistar rats. The use of these nanoparticles to treat antibiotic-resistant infections is promising given their high stability and cytocompatibility.



INTRODUCTION

Antibiotic-resistant (AR) bacteria and the lethal infections they can cause are a subject of public concern.^{1,2} Indeed, the World Health Organization has described antibiotic resistance as “a problem so serious that it threatens the achievements of modern medicine”.³ Thus, there is an urgent need for the development of novel strategies and drugs. In recent years, nanoparticles have been tested as potential antibacterial agents; particularly, gold nanoparticles (AuNPs) were chosen to act as photosensitizers because of their inert nature and effectiveness in spite of their polymorphism and polydispersity.⁴ Further, AuNP plasmons can absorb visible light,⁵ thus avoiding the use of highly energetic wavelengths that cause cell photodamage, proving useful for cancer treatment.⁶ Additionally, we have shown the photoinduced bactericidal properties of AuNPs utilizing green light, even on AR clinical strains.^{7–10} Thus, plasmon excitation of the AuNPs can produce highly reactive oxygen species (ROS) levels causing oxidative stress after 4 h of photodynamic antimicrobial chemotherapy (PACT), leading to bacterial death. Furthermore, in vitro studies suggest that these AuNPs are nontoxic for eukaryotic cells. These results

stimulated the present work to explore the selectivity toward prokaryotic cells in cell co-cultures and the biocompatibility and distribution of the particles in vivo.

Many in vivo studies on the biodistribution and toxic effects of AuNPs show that they are controlled by the nanomaterial size, shape, and coating.^{11–13} The limited pore size of the endothelial wall in the tissue is the primary delivery barrier for nanoparticles, but it also allows selective accumulation in certain tissues. When nanoparticles are administered through intraperitoneal (IP) or intravenous injection, a variety of serum proteins bind to their surface, which are recognized, internalized, and carried to the liver or spleen.¹⁴ It is known that the majority of the AuNPs after IP injection are distributed to the liver and spleen in 2–3 h¹⁵ and that AuNPs had a high blood-clearance rate being mostly distributed in the liver, followed by the spleen and lungs.¹⁶ No matter the pathway used, AuNPs seemed to migrate into the circulatory system first

Received: November 12, 2017

Accepted: January 17, 2018

Published: January 30, 2018

and subsequently distributed into tissues and organs, thus mainly distributed by passive targeting.¹⁷

It has been demonstrated that AuNPs can enhance their bactericidal properties when combined with antibiotics, such as vancomycin, aminoglycoside, and amoxicillin, among others.^{18–23} Amoxicillin is a β -lactam antibiotic²⁴ and, like other penicillins, binds to and inhibits the carboxypeptidase and transpeptidase enzymes that are required for peptidoglycan biosynthesis (Figure S1).²⁵ The nitrogen-containing β -lactam ring is designed to target the penicillin-binding membrane proteins, which are involved in the cross-linking of the bacterial cell wall. Interestingly, amoxicillin is capable of reducing Au(III) to Au(0) and stabilizing the resulting AuNPs due to high affinity of the amino groups to the gold surface.

Here, we present the one-pot synthesis of amoxicillin-coated AuNPs (amoxi@AuNPs) that combined to show enhanced photo-antimicrobial effect, i.e., highly reduced amount of antibiotic (typically 500 mg per dose are used), short irradiation time (\sim 30 min), and high selectivity toward prokaryotic cells. Facile-to-prepare amoxicillin-coated AuNPs were stable inside the bloodstream and tissue distribution, showing rapid clearance from the organism at the same time. In this sense, they are a better option for clinical use in comparison to other stabilizing agents, such as glutathione.²⁷ Furthermore, we introduce a novel method to check the selectivity of the toxicity in a co-culture of bacteria and blood cells through time-resolved fluorescence microscopy.

RESULTS AND DISCUSSION

Synthesis and Characterization of Amoxi@AuNPs.

AuNPs were synthesized by thermal reduction utilizing amoxicillin as both reducing and stabilizing agent. The absorption spectrum (Figure 1) of the amoxi@AuNPs shows

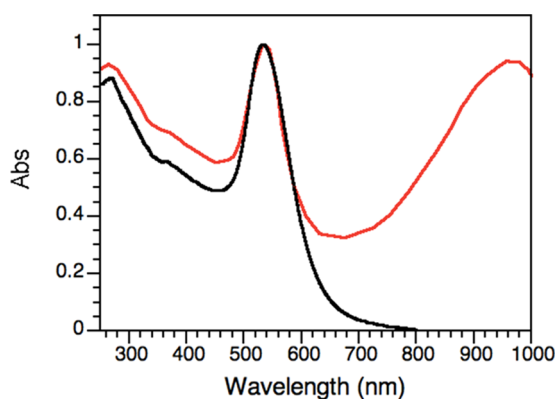


Figure 1. Normalized absorption spectra of unprotected AuNP (black) and of amoxi@AuNPs (red). The absorption wavelength at around 950 nm accounts for the presence of nonspherical nanostructures.

the characteristic plasmon band of small spherical nanoparticles centered around 540 nm, whereas the presence of a second absorption band around 950 nm can account for the plasmon absorption bands of more complex nanostructures, namely, triangular, hexagonal, and irregular polygonal plates, including nanorods (see Figures S2–S4).²⁸

Dynamic light scattering (DLS) measurements determined a hydrodynamic radius for the amoxi@AuNPs of 79 ± 43 nm. The broad distribution of particle sizes found by this technique is in agreement with the presence of larger nonspherical

nanostructures, in contrast to the AuNPs synthesized with NaBH_4 (“unprotected” AuNPs) that show a more monodisperse size distribution: 8 ± 2 nm. The positive ζ (Zeta) potential value found for amoxi@AuNPs ($+30 \pm 7$ mV) confirms the effectiveness of the amoxicillin as colloidal stabilizer.

The conjugation of the stabilizer agent to the nanoparticle was confirmed by Fourier transform infrared (FT-IR) spectroscopy (see Figure S5). AuNPs showed \sim 11% amoxicillin loading, as determined by thermogravimetric analysis (TGA). This amount is enough to stabilize the particle, but it is very low compared to the daily dose administered to a patient (1–2 g), which could minimize all of the amoxicillin side effects.^{29,30}

These new amoxi@AuNP composites showed great stability in different media, such as phosphate-buffered saline (PBS) 37.5, 25, 12.5, and 7.5% for 72 h; ceramide monohexoside (CMH) 25% for 48 h; CMH 12.5 and 7.5%; CTS 25, 12.5, and 7.5% for 168 h; and Milli-Q water for 96 h. (Figure S6). Nevertheless, they crashed immediately in all concentrated biological media and PBS (100 and 50%). On the basis of these findings, microbiological assays were carried out in 37.5% PBS, which allows the bacteria to be metabolically active and does not interfere with the monitoring of the plasmon absorption.

In Vitro Studies. Antibacterial Activity. *Staphylococcus aureus* ATCC 29213 (MSSA) and a methicillin-resistant clinical isolate of *S. aureus* (MRSA) were killed by 1.5 $\mu\text{g}/\text{mL}$ amoxi@AuNPs after only 30 min of irradiation (Figure 2) with white light using a light-emitting diode (LED) expo-panel (Figure S7). This is considerably faster than other nano-photosensitizers we have previously tested under similar exposure conditions.^{7,10} It is worth noting that light itself does not produce any damage or change of the bacterial normal growth. The selection of white light irradiation was based on the broad absorption spectrum shown by the amoxi@AuNPs composites (Figure 1), ensuring the excitation of most of the nanostructures present in the solution. Interestingly, excitation using only green light (525 nm) did not produce antibacterial effect; thus, the bactericidal effect requires the excitation of more complex nanostructures using the full visible spectrum. Additionally, amoxi@AuNPs were able to kill all of the MSSA after 90 min in the dark but not the MRSA. This could be a consequence of the synergistic effect^{18,31} between the antibiotic and the nanoparticle, as amoxicillin alone was not bactericidal at this low dose. It is important to highlight that the system temperature was kept at 37–38 $^\circ\text{C}$ during all of the experimental procedures. Despite the constant bulk temperature, it is well known that the excitation of the surface plasmon of AuNPs can induce a localized heat on the particle surface. Thus, the high local temperature experienced by the bacteria in close proximity to the surface of the particle could trigger their death.³² In fact, gold nanoparticles are able to convert the absorbed light into heat very efficiently. These results in a hot lattice and the temperature could increase up to tens of degrees, enough to denaturalize biomolecules.^{33–35}

ROS Quantification in Bacterial Culture. The generation of ROS was determined for samples of MRSA phototreated with amoxi@AuNP (at bactericidal concentrations). Figure 3 shows the maximum ROS production (almost 25 times basal level) quantified after just 10 min of irradiation. This level of ROS generation is even higher than the one observed for *S. aureus* treated with AuNP and light.¹⁰ A significant amount of ROS formation (almost 17 times basal level) can be formed after 30 min of irradiation, although no bacterial growth was observed at

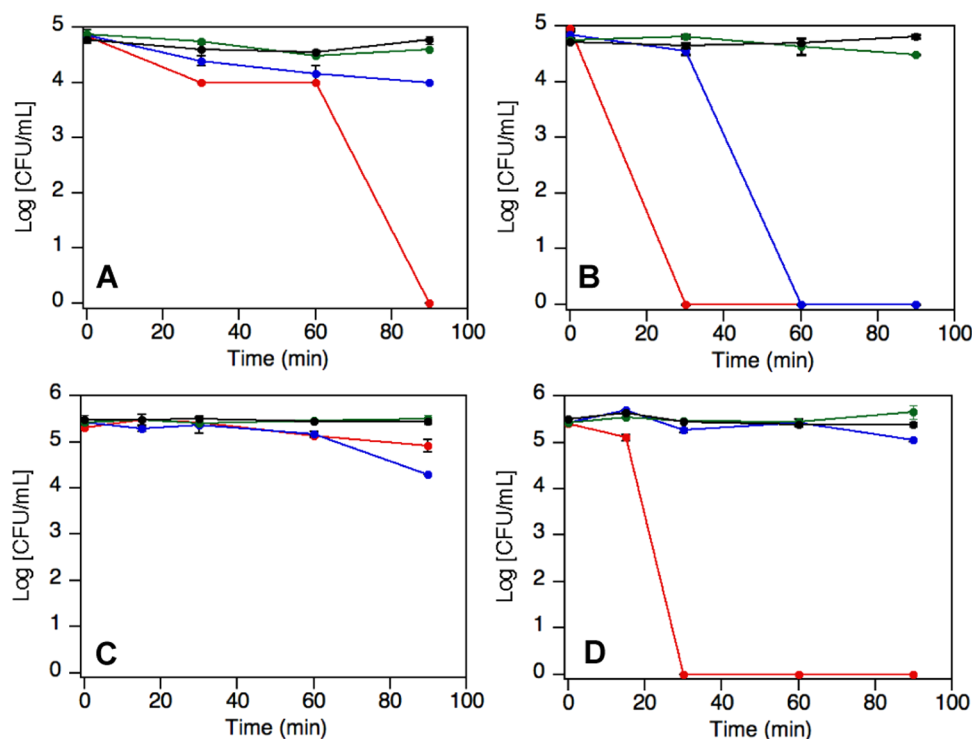


Figure 2. Bacterial growth over time of MSSA (A, B) and MRSA (C, D) samples treated under dark conditions (A–C) and under LED illumination (B–D) in the presence of 1.5 μg/mL of amoxi@AuNPs (red), 0.15 μg/mL amoxi@AuNPs (blue), and as control samples in the presence of amoxicillin at the minimum inhibitory concentration (MIC, green) or PBS (black). Note that unprotected AuNP at 10× concentration causes damage to the bacteria after 9–12 h of exposure to light (not shown).¹⁰

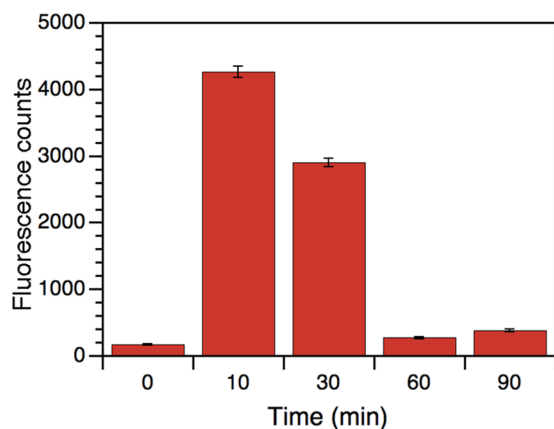


Figure 3. ROS production for samples of MRSA phototreated with amoxi@AuNP (at bactericidal concentrations).

that time. This could be due to the presence of some bacteria organelles and structures, whose global integrity and functionality are too damaged to keep bacteria alive. After 60 min, ROS production is negligible. Dark levels are almost null (not shown). The temperature of all of the samples (including the irradiated ones) was kept at 37 °C during the whole experiment, avoiding the influence of macroscopic thermal effect. This significant amount of ROS detected could indicate that the bactericidal effect is in direct relation with the oxidative stress generated in bacteria when amoxi@AuNP (attached to their wall) are irradiated.

Mammalian Cell Viability. The 3T3 cell line has become the standard fibroblast cell line since Todaro and Green originally obtained them from Swiss albino mouse embryo tissue in

1962.^{36,32} This line corresponds to immortalize cells; however, fibroblasts are much more sensitive to external factors than HeLa cells, most frequently used for in vitro experiments. For this reason, the activity of its mitochondrial enzymes, as evaluated by 3-(4,5-dimethylthiazol-2-yl)-2,5-diphenyltetrazolium bromide (MTT) assay, is an important parameter for the analysis of the effects of new drugs on eukaryotic cells, as it is a reflection of potential toxicity to mammals. Figure 4 shows the effect of free amoxicillin, unprotected AuNPs, and amoxi@AuNPs on their antibacterial or photo-antibacterial concentrations. Our results suggest that the cell viability of the samples

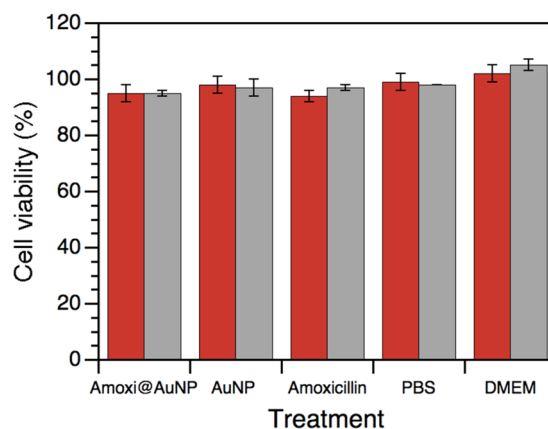


Figure 4. Cell survival (%) of fibroblast 3T3 treated with 1.5 μg/mL amoxi@AuNP, 2 μg/mL unprotected AuNP, 32 μg/mL amoxicillin, 37.5% PBS, and DMEM under 24 h visible light irradiation (red) and under dark conditions (gray) for 24 h at 37 °C, 5% CO₂, and 95% humidity.

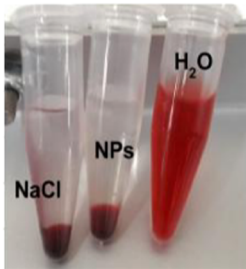
with antibiotic or nanoparticles is similar to control without drug (37.5% PBS), and they all presented slightly less survival than the control with Dulbecco's modified Eagle's medium (DMEM). Free amoxicillin was found to be nontoxic to other mammal cells in previous literature reports, whereas our own studies described the biocompatibility of uncoated AuNPs.^{10,37}

Figure 4 shows that amoxi@AuNPs were not cytotoxic even under the same irradiation conditions used for the antimicrobial test. Similar results were found for gold nanoparticles embedded in amphiphilic block copolymers.³⁸ AuNPs are essentially harmless compared to other antimicrobial nanoparticles, such as zinc nanoparticles, which have a substantial toxic impact on human fibroblast after 24 h.³⁹ This demonstrates that the proposed photosensitizer is selectively toxic for bacteria and does not affect eukaryotic cells to any significant extent, due to the absence of any penicillin-binding protein 1A on the eukaryotic membrane.

Parenteral and intraperitoneal injection of nanoparticles can produce high local concentration and broad distribution in the circulating blood, leading to the need for evaluation of their biological safety. Ex vivo experiments on whole blood were conducted because erythrocytes together with other blood cells and serum content reflect properly the actual conditions in mammals.⁴⁰ Experiments were performed at $t = 0, 2, 5,$ and 24 h in the dark and under LED irradiation, with the bactericidal concentration of amoxi@AuNP (1.5 $\mu\text{g}/\text{mL}$). Total hemolysis was established by adding H_2O to the red blood cell samples; $n = 3$; $\text{SD} < 0.1$ (see Figure S7 for illumination details). The tested amoxi@AuNPs did not produce any alteration to the red blood cells, as shown in Table 1. There was no hemolysis at all,

Table 1. Hemolysis Percentage (%) of Blood Samples Treated with 1.5 $\mu\text{g}/\text{mL}$ Amoxi@AuNP and with 0.9% NaCl as Negative Control and H_2O as Positive Control

T	Control		Amoxi@AuNPs	
0 h	1.3	1.2	1.2	1.3
2 h	1.3	1.3	1.3	1.4
5 h	1.2	1.2	1.2	1.2
24 h	1.3	1.2	1.2	0.9
LED	OFF	ON	OFF	ON



even under irradiation conditions. Thus, the amoxi@AuNPs are selectively toxic for bacteria and do not affect erythrocytes. Under these illumination conditions, the photothermal effect is then harmless for eukaryotic cells.

To further prove that amoxi@AuNPs are selectively toxic for bacteria, co-cultures with blood cells were treated with the particles under the same irradiation conditions. The fluorescence lifetime imaging microscopy (FLIM) technique is extremely useful in bioimaging, where, for instance, light scattering can interfere with steady-state fluorescence imaging. The fluorescence lifetime can change depending on the fluorophore environment and hence the same fluorophore can be tracked in different locations utilizing the same emission wavelength. Here, we use this technique together with a well-known DNA and RNA intercalator, acridine orange (AO-see Figure S8).⁴¹ Concentrations of AO around 0.3 mg/mL (1 mM) or higher lead to the formation of nonfluorescent dimers.⁴² However, AO can intercalate in nucleic acid helices as

the cationic monomer can presumably bind through electrostatic interaction with negatively charged phosphate. This interaction recovers the AO fluorescent properties and is the reason why AO is extensively used as a biological stain in fluorescence microscopy. When bound to ssDNA, AO shows a stable emission maximum at 630 nm upon excitation at around 458 nm. Interestingly, AO, when externally bound to disorganized or broken genetic material, is energetically less stable and is also very weakly emissive.⁴³ Here, AO was found to bind to the genetic material in both live bacteria and cells showing emission around 630 nm upon excitation at 440 nm. When the cells are subjected to damage, the genetic material of a dead cell is severely disrupted if not completely disintegrated. As a consequence, the AO most likely spreads into the solution as the nonfluorescent dimer forms or remains externally bound to the remaining DNA/RNA bases, producing a weak and short emission. Interestingly, the lifetime of the emissive structures is different when the AO is attached to live bacteria (ca. 3–7 ns), live white blood cells (ca. 7–14 ns), or bound externally to the disrupted genetic material of dying cells (<3 ns) with a lifetime almost as short as free AO.⁴⁴ Thus, using time-resolved fluorescence techniques, we were able to differentiate live bacteria or eukaryotic cells from dead ones.

According to the lifetime color scale at the bottom of Figure 5, groups of *S. aureus* appeared bright green when alive (Figure 5A) and the few dead coccus that are dead but were not completely broken by photothermal effect of PACT appeared blue (Figure 5B), indicating a decrease in the AO emission lifetime. Live erythrocytes (without nucleus or genetic material) were observed as pale green rings (Figure 5C–E) and were not found after heating the control sample (Figure 5F). The same sample presented a 98% of hemolysis in parallel measurements. Regarding eukaryotic cells with genetic material, lymphocytes, were observed as bright yellow-orange spots when alive (Figure 5C–E) and pale green spots when dying or damaged (Figure 5F). A larger white blood cell (eosinophil) was observed alive (Figure 5E). Its nucleus appeared dull green because of the lax chromatin content; however, the AO presented longer lifetimes, up to 14 ns in the cytoplasm, due its strong interaction with eosinophilic granules, described by Ueki et al.⁴⁵ and previously by Robbins et al.⁴⁶ The aforementioned difference in the emission lifetime of AO was developed as a practical and fast method to study the survival of both eukaryotic and prokaryotic cells together. It requires just one fluorescent dye, one excitation laser, and one emission filter, in contrast to other similar techniques that excite AO with different lasers and need other fluorescent dyes as ethidium bromide or propidium iodide as contrast agents.^{47,48}

In Vivo Studies. The distribution of the nanoparticles in internal organs is crucial to determine their in vivo stability and fate after the desired activity is completed. Following IP injection (see Experimental Section), amoxi@AuNPs were found using transmission electron microscopy (TEM) analysis (Figure 6) inside the liver (rows A and B), the kidney (rows C and D), and the spleen (rows E and F). Importantly, they did not go through the brain–blood barrier as amoxi@AuNPs were not found in brain tissue (data not shown). In general, the nanoparticles were internalized in vesicles in Kupffer cells in the liver just 2 h after IP injection. Usually, hepatobiliary system represents the main route of excretion for particles that do not undergo renal clearance.⁴⁹ Nanoparticles of diameter less than 100 nm, smaller than the pore size of liver fenestrae, could have easily penetrated through the endothelial wall too. At the same

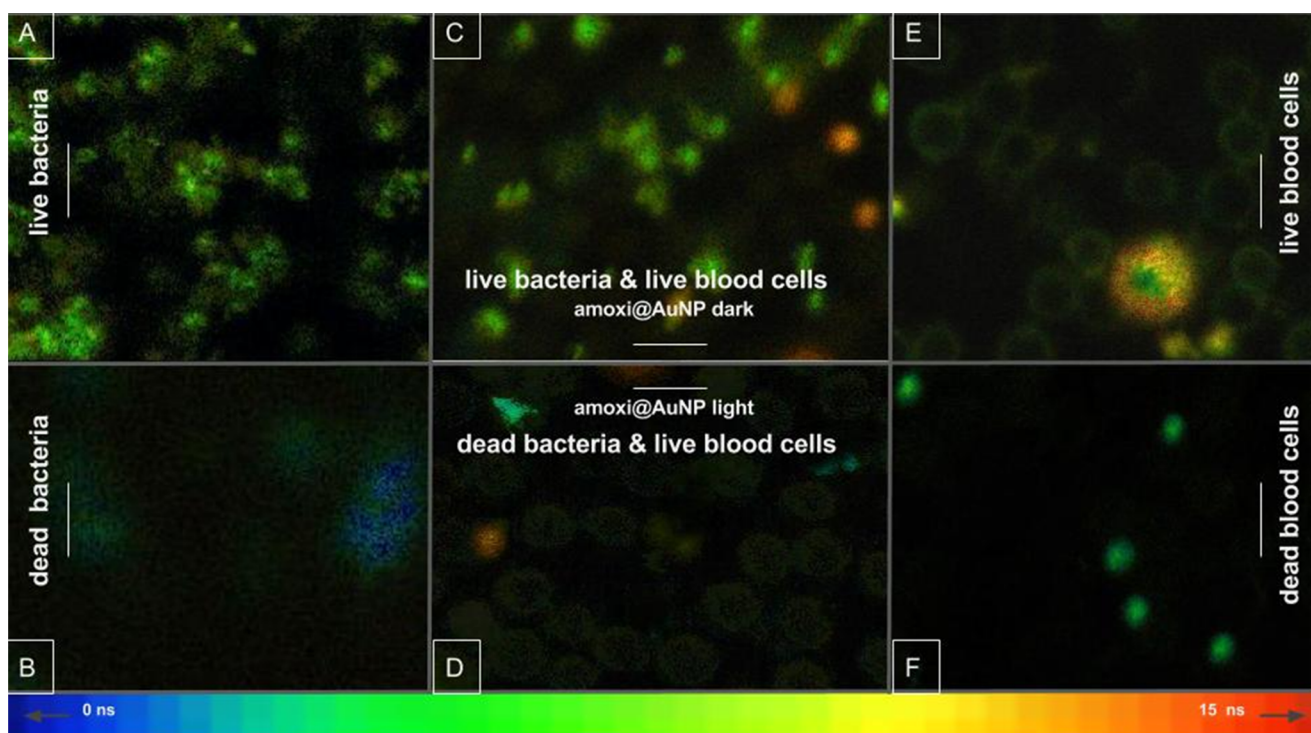


Figure 5. FLIM images of biological samples containing AO: co-culture of MSSA and blood cells treated with amoxi@AuNP for 30 min under dark conditions (C) and under irradiation (D); *S. aureus* suspension treated with amoxi@AuNP for 30 min under dark conditions (A) and under irradiation (B); blood cells treated with amoxi@AuNP for 30 min under dark conditions (E) and heated at 80 °C (F). Color gradient bar at the bottom indicates lifetime of AO emission in nanoseconds (ns). The scale bar is 20 μ m.

time, some amoxi@AuNPs were found in the spleen, indicating that they had been carried there earlier by the phagocytic cells. However, for these nanoparticles, our results indicate that the largest NP amount was found in the kidneys (2 h post injection) being internalized in vesicles after having gone through the microvilli. Only a small fraction of the nanoparticles was found in the samples taken 5 h after administration. This could be due to the elimination in urine (vide infra) or as a result of normal process of vesicle degradation because shrunken vesicles were observed (Figure 6IIC,D). In kidneys and the spleen, where a few nanoparticles were interacting with the dense chromatin, around 5% of pyknotic nuclei were observed ($n = 1008$ cells), possibly as a consequence of the oxidative stress generated by the nanomaterial.⁵⁰ It is noteworthy that after 24 h all three organs presented normal histopathology. Their different composing cells (including hepatocytes, epithelial and endothelial cells, podocytes, macrophages, and red and white blood cells) looked unaltered and were of normal size and structure. The AuNP without antibiotic stabilization were only found in small quantities in the liver at 2 h, indicating their poor stability in biological fluids after injection. According to our results, coating of AuNP is necessary to improve their in vivo stability. To obtain a global characterization, 2 grids were prepared for each organ (2 organs for each condition) and over 300 TEM pictures were taken. The more representative ones were selected to illustrate the path of the nanoparticles through the tissues studied (Figure 6).

Additionally, particles larger than the effective pore size in normal intact endothelium (5 nm), such as those used here, experience prolonged circulatory times due to slow transportation across the endothelium; therefore, the study of their effect on blood cells is quite relevant. Cell counting (Table 2)

on samples of rats injected with nanoparticles (groups I and II) was not different from the control animals (group III), except for a slight increase in the number of neutrophils (10% over top reference value, $p < 0.05$) in group II at 2 h. This is correlated with the observation of active phagocytic cells in the liver, kidneys, and spleen at the same time. The elevation in neutrophils may be due to the host response to the injection and distribution of amoxi@AuNPs. Normal values were totally restored after 24 h as a sign of complete elimination of the nanoparticles from the organism. According to microscope observation of smears, red blood cells from group I to II kept their integrity, suggesting that they were not stressed by the nanomaterial. This finding is in agreement with the ex vivo hemolysis test results.

Finally, renal excretion is the desirable pathway for AuNP removal because it would keep the catabolism or breakdown to a minimum, avoiding possible side effects.⁴⁹ Renal clearance as a fundamental part of drug elimination is determined by the molecular chemical and physical properties, including size, surface charge, and surface chemistry.⁵¹ Without such clearance or their biodegradation into biologically benign components, the toxicity potential increases. To address this concern, qualitative detection of intact nanoparticles in urine was done by measuring their plasmon absorption (Figure 7). Urine samples from group II showed an absorption peak ($abs < 0.40$) at 540 nm, consistent with spherical AuNP after 5 h of IP injection. Apparently, other shapes and sizes would preferably be uptaken by cells and degraded inside vesicles as shown in TEM pictures. It seems that most of the nanomaterial is being eliminated between 2 and 5 h after injection because the plasmon peaks are not bigger in urine samples collected 1 day after injection than in those collected 5 h after injection; in agreement with previous report.⁵² Both works suggest that the

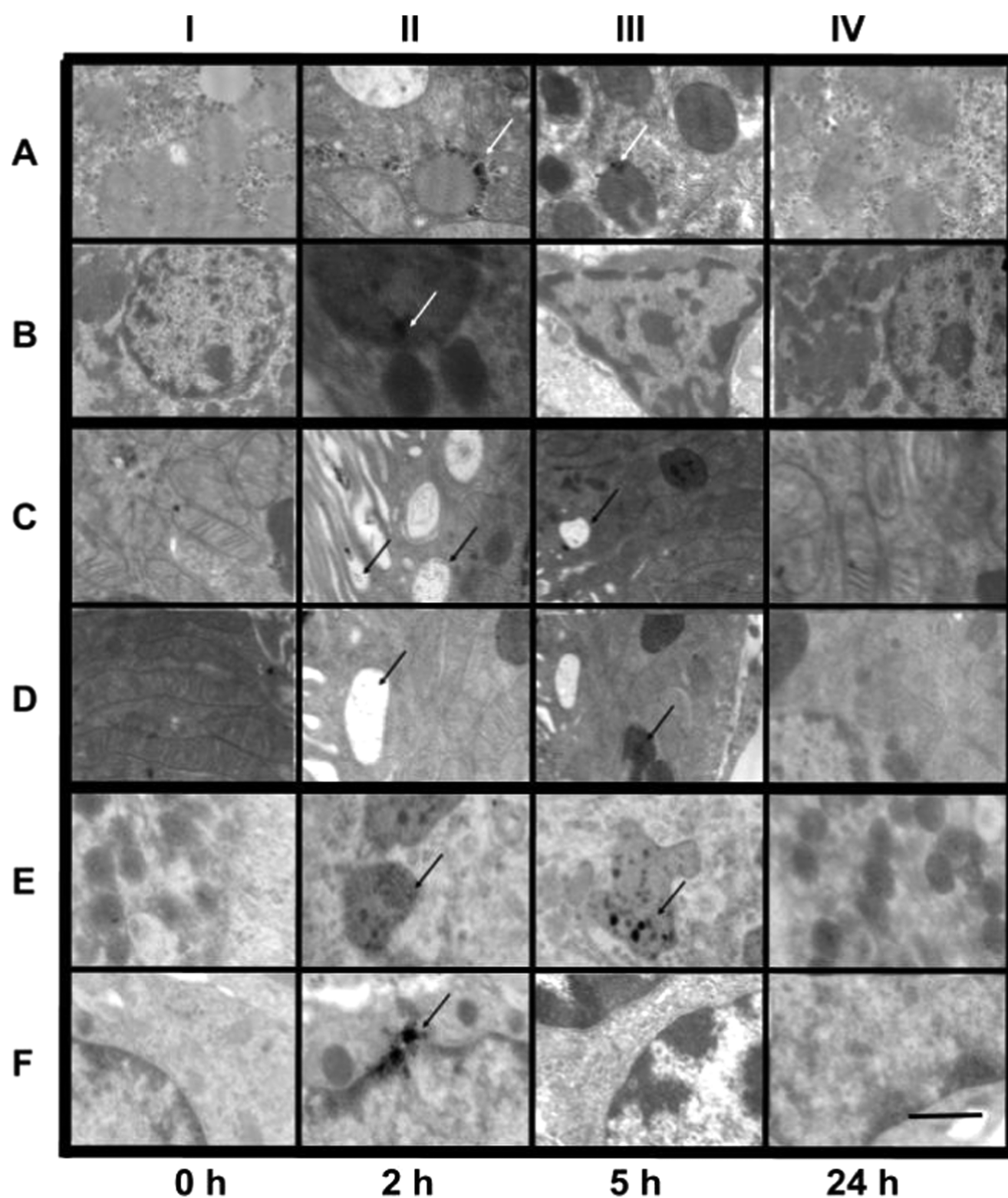


Figure 6. Representative TEM images of rat tissue samples showing the biodistribution of amoxi@AuNPs in the liver (rows A and B), kidneys (rows C and D), and spleen (rows E and F) after intraperitoneal injection. The scale bar is the same ($1 \mu\text{m}$) for all images.

kidneys are the primary sites for clearance of the smallest particles, followed by the hepatobiliary system. No unprotected AuNPs were found in urine collected from group I, supporting the hypothesis that uncoated AuNP are not being well distributed/eliminated. In summary, amoxicillin is beneficial not only for the stabilization of the nanoparticles but also for their renal clearance.

CONCLUSIONS

The combination of *in vivo* and *in vitro* studies presented here showed that amoxi@AuNPs are suitable nanostructures for PACT applications. amoxi@AuNPs can be easily synthesized in one pot utilizing amoxicillin as both reducing and stabilizing agent. The particles are stable in biological media and show

Table 2. Cell Counting (%) from Blood Smears of Rats Treated with AuNP (I), Amoxi@AuNP (II), and Physiological Saline Solution (III)

%	ref ^{a,b}	2 h			5 h			24 h		
		I	II	III	I	II	III	I	II	III
N	1–16	18	26	5	12	16	6	10	11	6
L	82–96	82	74	94	86	82	93	89	87	92
M	0–3	0	0	1	2	2	0	0	2	2
E	0–2	0	0	0	0	0	1	1	0	0
B	0	0	0	0	0	0	0	0	0	0
SN	0–1	0	0	0	0	0	0	0	0	0

^a“ref” are the reference values for healthy male Wistar rats. ^bN (neutrophils), L (lymphocytes), M (monocytes), E (eosinophils), B (basophils), SN (segmented neutrophils).

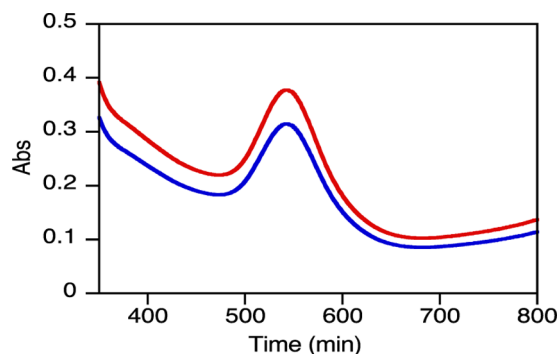


Figure 7. Absorption spectra of amoxi@AuNPs from rat urine collected 5 h (blue) and 24 h (red) after IP injection and resuspended in 37.5% PBS.

photoinduced antibacterial activity (irradiation time \sim 30 min), even against AR strains. Importantly, amoxi@AuNPs are very biocompatible with eukaryotic cells under PACT conditions. The bacterial death is believed to occur upon localized surface plasmon excitation of the AuNP. The antibiotic was used as a reducing agent for the synthesis of AuNPs, and its presence confers the NP with the selectivity toward the bacterial cell. This is a major advantage when combating microorganism that produce lytic enzymes, developing antibiotic resistance. Accordingly, the amoxi@AuNPs can act faster than silver and zinc nanoparticles tested by other groups without plasmon excitation,⁵³ showing their potential as antibacterial agents.

We have also demonstrated that FLIM can be very useful to determine the cell selectivity and bactericidal activity in prokaryotic/eukaryotic co-cultures by a rapid and simple analysis. This analysis only requires one fluorescent dye, one excitation laser, and one emission filter, in contrast to similar techniques that excite AO with different lasers and need other fluorescent dyes as ethidium bromide or propidium iodide as contrast agents.

Finally yet importantly, our results show that the injected AuNPs have a higher clearance rate than other similar nanomaterials^{54,55} and have not induced considerable cytotoxicity responses. As a result, amoxi@AuNPs seem to have a low potential of accumulation in mammals. These findings are remarkably useful for the potential development of pharmaceutical formulations.

EXPERIMENTAL SECTION

Materials. Tetrachloroauric acid-99% (HAuCl₄) was purchased from Sigma-Aldrich, and trihydrate amoxicillin was purchased from Todo Droga (Argentina). Mueller Hinton

broth (MHB), tryptic soy broth (TSB), tryptic soy agar (TSA), brain heart infusion, Luria Bertani broth, and phosphate-buffered saline (PBS) were purchased from Britania (Argentina).

Synthesis of Amoxi@AuNPs and AuNP. Antibiotic-coated nanoparticles were prepared with amoxicillin in a one-step synthesis using the antibiotic as both the reducing and stabilizer agent. This bottom-up method is based on the reduction of the gold precursor (HAuCl₄ 100 μ L, 10 mM) with amoxicillin trihydrate (900 μ L, 0.1 mM) at 50 $^{\circ}$ C for 18 min. This corresponds to a 16 wt % of amoxicillin with respect to the mass of Au. All solutions were freshly prepared prior to the synthesis and left to stabilize at room temperature for 30 min before heating. Three cycles of Milli-Q water washing and centrifugation were used to remove unbound amoxicillin molecules.

To obtain 500 mL of 0.2 mM unprotected AuNP, 1 mL of 0.1 M HAuCl₄ aqueous solution was added to 500 mL of previously cooled Milli-Q water (8 $^{\circ}$ C). Then, 10 mL of a NaBH₄ (0.13 M) solution was transferred dropwise to the flask.

Characterization of Amoxi@AuNP. The changes of the surface plasmon resonance of the resuspended pellet and the absorption spectrum of the amoxicillin molecules present in the supernatant were monitored using a Cary 60 UV–vis spectrophotometer. The shape and size of the synthesized AuNP were measured by transmission electron microscopy (TEM-Jeol 1200 EX II). Samples for TEM measurements were prepared by placing a 4 μ L drop of the amoxi@AuNP solution on carbon-coated copper grids and left to dry completely at 37 $^{\circ}$ C in a drying oven. At least 400 nanoparticles were analyzed statistically using ImageJ software. On the same samples, ζ potential and dynamic light scattering (DLS) were measured with a Malvern Zetasizer (model Nano-S). The binding of amoxicillin to AuNP was analyzed by a Fourier transform infrared (FT-IR) spectrometer in transmission mode using a Nicolet iN 10 spectrophotometer. Samples of amoxicillin trihydrate, unprotected AuNP, and amoxi@AuNPs were freeze-dried and then measured by FT-IR at low temperature.

The amount of amoxicillin was determined by thermogravimetric analysis (TGA). For this, 4 mL of 1.5 μ g/mL of the amoxi@AuNPs were centrifuged down and pellets were combined to be exhaustively dried in a desiccator for 48 h prior to TGA at 10 $^{\circ}$ C/min from 25 to 1000 $^{\circ}$ C under nitrogen atmosphere (flow rate of 25 mL/min) with a TA-THA Q5000. The TGA curves were used to determine the amoxicillin amount attached to AuNP by extrapolating the weight loss values from the y-axis.

Colloidal Stability. Stability measurements of amoxi@AuNPs (1.5 μ g/mL) in different buffer solutions and growth

media were conducted on the basis of the change in plasmon absorbance maxima at different time points, utilizing UV–vis spectrophotometry. Stability was considered as the time it took for a 20% decrease in plasmon absorption at the wavelength of the initial maximum absorbance.⁸ The stability measurements were carried out (using a BioTek plate reader) for 7 days (time = 0, 0.5, 1, 2, 4, 6, 12, 18, 24, 48, 72, 120, 144, 168 h) in Milli-Q water, saline solution, PBS (pH = 7), Mueller Hinton broth (MHB), and tryptic soy broth (TSB) at different concentrations (100, 50, 25, 12.5%). To avoid contamination, the stability measurement of nanoparticles dispersed in growth media was conducted under sterile conditions.

Bacterial Strains and Growth Conditions. The experiments were performed using *S. aureus* ATCC 29213 (MSSA ATCC 29213) and a methicillin-resistant clinical isolate of *S. aureus* (MRSA 9455). Clinical isolate was supplied by the Bacteriology Service of Sanatorio Aconcagua, Córdoba, Argentina. Stock cultures were maintained in TSB and stored in a freezer in 10% glycerol.

Antibacterial Capacity. Antibacterial activity of novel amoxi@AuNPs against MSSA and MRSA was tested. Bacterial suspensions of 10^6 colony-forming units per milliliter (CFU/mL) in 37.5% PBS (pH = 7) from a single colony of each strain were prepared. Using a 96-well plate, 100 μ L of bacterial suspension and 100 μ L of the tested solutions (37.5% PBS, 0.15 μ g/mL, amoxi@AuNPs, 1.5 μ g/mL amoxi@AuNPs, and amoxicillin at minimum inhibitory concentration (MIC) per strain as control: 2 μ g/mL for MSSA and 32 μ g/mL for MRSA) were mixed and irradiated for a total of 90 min under white LED illumination at 37 °C. Control experiments were run under the same conditions in the dark. All samples were run in triplicate. Aliquots of each sample were diluted properly and seeded in TSA plates. CFUs were counted from the agar after 24 h of incubation at 37 °C.

ROS Quantification in Bacterial Culture. The prefluorescent probe dihydrorhodamine 123 (DHR) was chosen for its high sensitivity to quantify total ROS and reactive nitrogen species.⁵⁶ This dye diffuses passively through most of cell membranes, where DHR generates a fluorescent green signal at 536 nm when oxidized. Radical indicators of oxidative stress were measured with DHR (1 μ M) in bacterial suspensions (109 CFU/mL) treated with a 1.5 μ g/mL of amoxi@AuNPs. The samples were irradiated for 10, 30, 60, and 90 min.

Cell Viability. The 3T3 fibroblasts were cultured in Dulbecco's modified Eagle's medium (DMEM) with 10% calf serum. Cells were grown until 85–95% confluence, then washed with phosphate-buffer saline (Invitrogen), and trypsinized with 1 mL of 0.05% trypsin, 0.53 mM ethylenediaminetetraacetic acid, phenol red. Trypsinization was stopped by adding fresh medium to the reaction. The cells were washed twice by centrifugation with DMEM without serum, resuspended in medium without serum, and plated at approximately 10^5 cells per well after proper cell counting in an improved Neubauer chamber. They were incubated overnight to allow attachment and then treated with 1.5 μ g/mL amoxi@AuNP, 32 μ g/mL amoxicillin, 37.5% PBS, and DMEM and irradiated with a white LED for 24 h. The cells were kept in the dark for 24 h at 37 °C, 5% CO₂, and 95% humidity. MTT assay based on the reduction of tetrazolium salt to formazan crystals in living cells was done according to a Sigma protocol to determine the percent survival.⁵⁷ The absorbance spectra on the different wells were measured using a BioTek plate reader.

Hemolysis. The integrity of red blood cells from human healthy volunteers (from Córdoba, Argentina) incubated with amoxi@AuNPs 1.5 μ g/mL with and without irradiation was evaluated following a procedure previously described⁵⁸ with slight modifications. The amoxi@AuNPs had to be removed by centrifuging the samples before reading the absorbance of the free hemoglobin (541 nm) to avoid spectral interference. Measurements were made at 0, 2, 5, and 24 h in triplicate. An aqueous solution of 0.9% NaCl and H₂O were used as negative and positive controls of hemolysis, respectively.

Fluorescence Lifetime Imaging Microscopy (FLIM) Study on Co-cultures of Blood Cells and Bacteria.

Acridine orange (AO) was employed due to its characteristic fluorescence emission when intercalated in DNA or RNA.^{59,60} FLIM imaging of the dye was introduced as a method to check the viability of blood cells (anticoagulated fresh samples from healthy volunteers from University of Córdoba) and bacteria (10^7 CFU/mL of *S. aureus* 29213) cultured together and treated with irradiated and nonirradiated amoxi@AuNPs (1.5 μ g/mL). The samples were studied using a fluorescent lifetime imaging system (FLIM, PicoQuant MicroTime 200). The instrument was equipped with a frequency-doubled picosecond pulse diode laser (440 \pm 10 nm, 70 ps, 40 MHz, LDH-D-C-440, PicoQuant). The laser beam was collimated and focused through a fiber-coupling unit. A beam splitter Z440 bcm (Chroma) was used to reflect the excitation light into the oil immersion total internal reflection objective (100 \times , NA1.45, Olympus, PLAPO). The excitation dose (average power) is about 0.6 mW for all samples. Emission was collected between 610 and 680 nm using the ET645/75BP emission filter. Briefly, 100 μ L of the biological sample and 100 μ L of AO (1 mg/mL) were mixed and incubated at room temperature for 5 min. Lifetimes longer than 5 ns were found for live bacteria and cells, whereas dead bacteria or cells can be detected by a decrease in the emission intensity and lifetime of unbound AO produced by disorganization of the spread genetic material in necrotic or broken cells. Aliquots of the dye alone or mixed with amoxi@AuNPs were also tested for fluorescence. Fresh samples of blood cells or PBS suspension of bacteria in the absence of nanoparticles were run as controls for “alive samples”. Accordingly, the same samples were also heated up to 80 °C and imaged as “dead samples control”. Furthermore, bacterial growth in the observed samples was also ruled out by CFU counting in MH agar plates, whereas integrity of eukaryotic cells was monitored by parallel hemolysis measures.

Biodistribution of Nanoparticles. Male Wistar rats with a body weight of 280–310 g at the time of drug administration were maintained in the animal house facility at the Departamento Farmacología, Córdoba, Argentina (food and water provided ad libitum at a constant temperature of 22 \pm 2 °C with 12 h by 12 h light and dark cycle). The rats were handled for 1 week for acclimatization. At the beginning, the rats were divided into three groups of two rats each: group I was subjected to intraperitoneal injection with 34 μ g/mL AuNP, group II with 1.5 μ g/mL amoxi@AuNPs, and group III with physiological saline solution as control. After 2, 5, and 24 h post injection, two animals from each group were anesthetized using a mixture of 55 mg/kg ketamine and 11 mg/kg xylazine. Immediately, cardiac perfusion with PBS (0.1 M) was carried out to remove all red blood cells from their internal organs. Finally, after proper fixation (35 min perfusion with 2% paraformaldehyde and 2% glutaraldehyde in PBS), the liver, heart, kidney, spleen, and brain were harvested. TEM images

were taken with a TEM-Zeiss-Leo 906E microscope. All experiments on animals were conducted complying with the ARRIVE guidelines and were carried out in accordance with the National Institutes of Health Guide for the Care and Use of Laboratory Animals (NIH Publications No. 8023, revised 1978) and the Guide for the Care and Use of Laboratory Animals (Eighth Edition, 2011).⁶¹

Biocompatibility with Blood Cells. Prior to perfusion, blood smears (triplicates) were made from fresh blood extracted through a cardiac puncture.⁶² Samples were stained with May Grunwald/Giemsa and analyzed under an optical microscope. Results reported are the averages of quadruplicates. Student *t*-test was performed to detect differences that were considered statistically significant when *P* values were lower than $\alpha = 0.05$.

Renal Clearance. At the same time intervals (2, 5, and 24 h), urine was collected using metabolic boxes. The plasmon absorption of the AuNP was measured by spectroscopy using a multiwell spectrophotometer (BioTek), by centrifuging the collected urine and resuspending the pellet in 0.5 mL of 37.5% PBS.

■ ASSOCIATED CONTENT

📄 Supporting Information

The Supporting Information is available free of charge on the ACS Publications website at DOI: 10.1021/acsomega.7b01779.

Details of the experimental procedures, IR spectra, TEM images, and size distribution graphs (PDF)

■ AUTHOR INFORMATION

Corresponding Authors

*E-mail: becerra@fcq.unc.edu.ar (M.C.B.).

*E-mail: titoscaiano@mac.com (J.C.S.).

ORCID

Anabel E. Lanterna: 0000-0002-6743-0940

Juan C. Scaiano: 0000-0002-4838-7123

Author Contributions

All authors have approved the final article.

Funding

This work was supported in Argentina by grants from CONICET (PIP 2012-2014) grant no. 11220110100965, SECyT-UNC, and FONCyT (PICT 2014) grant no. 821 to Dr. Becerra, SECyT-UNC to Dr. Perez and in Canada thanks to the Natural Sciences and Engineering Research Council of Canada through its Discovery programs and the Canada Research Chairs program. MCB and MFP are career research members of CONICET. MJSC is especially grateful to CONICET for the postdoctoral fellowship and the scholarship awarded to visit the University of Ottawa. DMR and EAV have doctoral fellowships from SECyT-UNC.

Notes

The authors declare no competing financial interest.

■ ACKNOWLEDGMENTS

The authors are grateful to Estela Salde and Lorena Mercado for their laboratory technical assistance with the in vivo experiments and to Dr. Cristina Maldonado for her help in TEM samples preparation and analysis.

■ REFERENCES

- (1) Lutgring, J. D.; Granados, C. A. D.; McGowan, J. E. Antimicrobial Resistance: An International Public Health Problem. In *Antimicrobial Drug Resistance: Clinical and Epidemiological Aspects*; Mayers, D. L., Sobel, J. D., Ouellette, M., Kaye, K. S., Marchaim, D., Eds.; Springer International Publishing: Cham, 2017; Vol. 2, pp 1519–1528.
- (2) Spellberg, B.; Guidos, R.; Gilbert, D.; Bradley, J.; Boucher, H. W.; Scheld, W. M.; Bartlett, J. G.; Edwards, J. J. The Epidemic of Antibiotic-Resistant Infections: A Call to Action for the Medical Community from the Infectious Diseases Society of America. *Clin. Infect. Dis.* **2008**, *46*, 155–164.
- (3) WHO. Antimicrobial Resistance: Global Report on Surveillance, 2014; p 257.
- (4) Suresh, A. K. *Metallic Nanocrystallites and Their Interaction with Microbial Systems*; Springer: Dordrecht, 2012; p 67.
- (5) Bucharskaya, A.; Maslyakova, G.; Terentyuk, G.; Yakunin, A.; Avetisyan, Y.; Bibikova, O.; Tuchina, E.; Khlebtsov, B.; Khlebtsov, N.; Tuchin, V. Towards Effective Photothermal/Photodynamic Treatment Using Plasmonic Gold Nanoparticles. *Int. J. Mol. Sci.* **2016**, *17*, No. 1295.
- (6) Huang, X.; El-Sayed, I. H.; Qian, W.; El-Sayed, M. A. Cancer cell imaging and photothermal therapy in the near-infrared region by using gold nanorods. *J. Am. Chem. Soc.* **2006**, *128*, 2115–2120.
- (7) Fasciani, C.; Silvero, M. J.; Anghel, M. A.; Arguello, G. A.; Becerra, M. C.; Scaiano, J. C. Aspartame-Stabilized Gold-Silver Bimetallic Biocompatible Nanostructures with Plasmonic Photothermal Properties, Antibacterial Activity, and Long-Term Stability. *J. Am. Chem. Soc.* **2014**, *136*, 17394–17397.
- (8) de Alwis Weerasekera, H.; Silvero, M. J.; da Silva, D. R. C.; Scaiano, J. C. A database on the stability of silver and gold nanostructures for applications in biology and biomolecular sciences. *Biomater. Sci.* **2017**, *5*, 89–97.
- (9) Silvero, M. J.; Argüello, G. A.; Becerra, M. C. Photodynamic Antibacterial Chemotherapy (PACT) Using Gold Nanoparticles and LED's Irradiation. *J. Nanopharm. Drug Deliv.* **2014**, *2*, 148–152.
- (10) Silvero, M. J.; Becerra, M. C. Plasmon-induced oxidative stress and macromolecular damage in pathogenic bacteria. *RSC Adv.* **2016**, *6*, 100203–100208.
- (11) Shi, X. L.; Zhu, Y. T.; Hua, W. D.; Ji, Y. L.; Ha, Q.; Han, X. X.; Liu, Y.; Gao, J. W.; Zhang, Q.; Liu, S. D.; Ren, K. L.; Wu, X. C.; Li, H. Y.; Han, D. An in vivo study of the biodistribution of gold nanoparticles after intervaginal space injection in the tarsal tunnel. *Nano Res.* **2016**, *9*, 2097–2109.
- (12) Khlebtsov, N.; Dykman, L. Biodistribution and toxicity of engineered gold nanoparticles: a review of in vitro and in vivo studies. *Chem. Soc. Rev.* **2011**, *40*, 1647–1671.
- (13) Aydin, A.; Sipahi, H.; Charehsaz, M. Nanoparticles Toxicity and Their Routes of Exposures. In *Recent Advances in Novel Drug Carrier Systems*; Sezer, A. D., Ed.; InTech: Rijeka, 2012; Chapter 18.
- (14) Opanasopit, P.; Nishikawa, M.; Hashida, M. Factors affecting drug and gene delivery: Effects of interaction with blood components. *Crit. Rev. Ther. Drug Carrier Syst.* **2002**, *19*, 191–233.
- (15) De Jong, W. H.; Hagens, W. I.; Krystek, P.; Burger, M. C.; Sips, A. J. A. M.; Geertsma, R. E. Particle size-dependent organ distribution of gold nanoparticles after intravenous administration. *Biomaterials* **2008**, *29*, 1912–1919.
- (16) Wang, L.; Li, Y. F.; Zhou, L. J.; Liu, Y.; Meng, L.; Zhang, K.; Wu, X. C.; Zhang, L. L.; Li, B.; Chen, C. Y. Characterization of gold nanorods in vivo by integrated analytical techniques: their uptake, retention, and chemical forms. *Anal. Bioanal. Chem.* **2010**, *396*, 1105–1114.
- (17) Sharifi, S.; Behzadi, S.; Laurent, S.; Forrest, M. L.; Stroeve, P.; Mahmoudi, M. Toxicity of nanomaterials. *Chem. Soc. Rev.* **2012**, *41*, 2323–2343.
- (18) Gu, H. W.; Ho, P. L.; Tong, E.; Wang, L.; Xu, B. Presenting vancomycin on nanoparticles to enhance antimicrobial activities. *Nano Lett.* **2003**, *3*, 1261–1263.

- (19) Kalita, S.; Kandimalla, R.; Sharma, K. K.; Katak, A. C.; Deka, M.; Kotoky, J. Amoxicillin functionalized gold nanoparticles reverts MRSA resistance. *Mater. Sci. Eng., C* **2016**, *61*, 720–727.
- (20) Grace, A. N.; Pandian, K. Antibacterial efficacy of aminoglycosidic antibiotics protected gold nanoparticles - A brief study. *Colloids Surf., A* **2007**, *297*, 63–70.
- (21) Brown, A. N.; Smith, K.; Samuels, T. A.; Lu, J.; Obare, S. O.; Scott, M. E. Nanoparticles Functionalized with Ampicillin Destroy Multiple-Antibiotic-Resistant Isolates of *Pseudomonas aeruginosa* and *Enterobacter aerogenes* and Methicillin-Resistant *Staphylococcus aureus*. *Appl. Environ. Microbiol.* **2012**, *78*, 2768–2774.
- (22) Mu, H.; Tang, J.; Liu, Q.; Sun, C.; Wang, T.; Duan, J. Potent Antibacterial Nanoparticles against Biofilm and Intracellular Bacteria. *Sci. Rep.* **2016**, *6*, No. 18877.
- (23) Payne, J. N.; Waghwan, H. K.; Connor, M. G.; Hamilton, W.; Tockstein, S.; Moolani, H.; Chavda, F.; Badwaik, V.; Lawrenz, M. B.; Dakshinamurthy, R. Novel Synthesis of Kanamycin Conjugated Gold Nanoparticles with Potent Antibacterial Activity. *Front. Microbiol.* **2016**, *7*, No. 607.
- (24) Neu, H. C. Clinical Use of the Quinolones. *Lancet* **1987**, *2*, 1319–1322.
- (25) Hauser, A. R. *Antibiotic Basics for Clinicians: Choosing the Right Antibacterial Agent*; Wolters Kluwer: Philadelphia, 2007.
- (26) Fouladgar, M.; Hadjmohammadi, M. R.; Khalilzadeh, M. A.; Biparva, P.; Teymoori, N.; Beitollah, H. Voltammetric Determination of Amoxicillin at the Electrochemical Sensor Ferrocenedicarboxylic Acid Multi Wall Carbon Nanotubes Paste Electrode. *Int. J. Electrochem. Sci.* **2011**, *6*, 1355–1366.
- (27) Simpson, C. A.; Salleng, K. J.; Cliffel, D. E.; Feldheim, D. L. In vivo toxicity, biodistribution, and clearance of glutathione-coated gold nanoparticles. *Nanomedicine* **2013**, *9*, 257–263.
- (28) Kelly, K. L.; Coronado, E.; Zhao, L. L.; Schatz, G. C. The Optical Properties of Metal Nanoparticles: The Influence of Size, Shape, and Dielectric Environment. *J. Phys. Chem. B* **2003**, *107*, 668–677.
- (29) Gillies, M.; Ranakusuma, A.; Hoffmann, T.; Thorning, S.; McGuire, T.; Glasziou, P.; Del Mar, C. Common harms from amoxicillin: a systematic review and meta-analysis of randomized placebo-controlled trials for any indication. *Can. Med. Assoc. J.* **2015**, *187*, E21–E31.
- (30) Schrag, S. J.; Pena, C.; Fernandez, J.; Sanchez, J.; Gomez, V.; Perez, E.; Feris, J. M.; Besser, R. E. Effect of short-course, high-dose amoxicillin therapy on resistant pneumococcal carriage - A randomized trial. *J. Am. Med. Assoc.* **2001**, *286*, 49–56.
- (31) Smekalova, M.; Aragon, V.; Panacek, A.; Pucek, R.; Zboril, R.; Kvittek, L. Enhanced antibacterial effect of antibiotics in combination with silver nanoparticles against animal pathogens. *Vet. J.* **2016**, *209*, 174–179.
- (32) Huang, X.; El-Sayed, M. A. Gold nanoparticles: Optical properties and implementations in cancer diagnosis and photothermal therapy. *J. Adv. Res.* **2010**, *1*, 13–28.
- (33) St Denis, T. G.; Huang, L. Y.; Dai, T. H.; Hamblin, M. R. Analysis of the Bacterial Heat Shock Response to Photodynamic Therapy-mediated Oxidative Stress. *Photochem. Photobiol.* **2011**, *87*, 707–713.
- (34) Zhu, Y.; Ramasamy, M.; Yi, D. K. Antibacterial Activity of Ordered Gold Nanorod Arrays. *ACS Appl. Mater. Interfaces* **2014**, *6*, 15078–15085.
- (35) Ramasamy, M.; Lee, S. S.; Yi, D. K.; Kim, K. Magnetic, optical gold nanorods for recyclable photothermal ablation of bacteria. *J. Mater. Chem. B* **2014**, *2*, 981–988.
- (36) Leibiger, C.; Kosyakova, N.; Mkrtchyan, H.; Gleib, M.; Trifonov, V.; Liehr, T. First Molecular Cytogenetic High Resolution Characterization of the NIH 3T3 Cell Line by Murine Multicolor Banding. *J. Histochem. Cytochem.* **2013**, *61*, 306–312.
- (37) Amoxicillin, <https://www.drugbank.ca/drugs/DB01060> (accessed July, 2017).
- (38) Wijesiri, N.; Ozkaya-Ahmadov, T.; Wang, P.; Zhang, J.; Tang, H.; Yu, X.; Ayres, N.; Zhang, P. Photodynamic Inactivation of Multidrug-Resistant *Staphylococcus aureus* Using Hybrid Photosensitizers Based on Amphiphilic Block Copolymer-Functionalized Gold Nanoparticles. *ACS Omega* **2017**, *2*, 5364–5369.
- (39) Dönmez Güngüneş, Ç.; Şeker, Ş.; Elçin, A. E.; Elçin, Y. M. A comparative study on the in vitro cytotoxic responses of two mammalian cell types to fullerenes, carbon nanotubes and iron oxide nanoparticles. *Drug Chem. Toxicol.* **2017**, *40*, 215–227.
- (40) Aseichev, A. V.; Azizova, O. A.; Beckman, E. M.; Skotnikova, O. I.; Dudnik, L. B.; Shcheglovitova, O. N.; Sergienko, V. I. Effects of Gold Nanoparticles on Erythrocyte Hemolysis. *Bull. Exp. Biol. Med.* **2014**, *156*, 495–498.
- (41) Miao, Y.; Li, Y. T.; Zhang, Z. F.; Yan, G. Q.; Bi, Y. “Turn off-on” phosphorescent biosensors for detection of DNA based on quantum dots/acridine orange. *Anal. Biochem.* **2015**, *475*, 32–39.
- (42) Blears, D. J.; Danyluk, S. S. A Nuclear Magnetic Resonance Investigation of Aggregation of Acridine Orange in Aqueous Solution. *J. Am. Chem. Soc.* **1967**, *89*, 21–26.
- (43) Kubota, Y.; Steiner, R. F. Fluorescence Decay and Quantum Yield Characteristics of Acridine-Orange and Proflavine Bound to DNA. *Biophys. Chem.* **1977**, *6*, 279–289.
- (44) Nagata, S. DNA degradation in development and programmed cell death. *Annu. Rev. Immunol.* **2005**, *23*, 853–875.
- (45) Ueki, S.; Konno, Y.; Takeda, M.; Moritoki, Y.; Hirokawa, M.; Matsuwaki, Y.; Honda, K.; Ohta, N.; Yamamoto, S.; Takagi, Y.; Wada, A.; Weller, P. F. Eosinophil extracellular trap cell death-derived DNA traps: Their presence in secretions and functional attributes. *J. Allergy Clin. Immunol.* **2016**, *137*, 258–267.
- (46) Robbins, E.; Marcus, P. I. Dynamics of Acridine Orange-Cell Interaction. I. Interrelationships of Acridine Orange Particles and Cytoplasmic Reddening. *J. Cell Biol.* **1963**, *18*, 237–250.
- (47) Mansour, J. D.; Schram, J. L.; Schulte, T. H. Fluorescent Staining of Intracellular and Extracellular Bacteria in Blood. *J. Clin. Microbiol.* **1984**, *19*, 453–456.
- (48) Frey, T. Nucleic-Acid Dyes for Detection of Apoptosis in Live Cells. *Cytometry* **1995**, *21*, 265–274.
- (49) Longmire, M.; Choyke, P. L.; Kobayashi, H. Clearance properties of nano-sized particles and molecules as imaging agents: considerations and caveats. *Nanomedicine* **2008**, *3*, 703–717.
- (50) Sutariya, V. B.; Pathak, Y. *Biointeractions of Nanomaterials*; CRC Press, 2014.
- (51) Kumari, A.; Yadav, S. K.; Yadav, S. C. Biodegradable polymeric nanoparticles based drug delivery systems. *Colloids Surf., B* **2010**, *75*, 1–18.
- (52) Hainfeld, J. F.; Slatkin, D. N.; Focella, T. M.; Smilowitz, H. M. Gold nanoparticles: a new X-ray contrast agent. *Br. J. Radiol.* **2006**, *79*, 248–253.
- (53) Hernández-Sierra, J. F.; Ruiz, F.; Pena, D. C. C.; Martínez-Gutiérrez, F.; Martínez, A. E.; Guillen, A. D. P.; Tapia-Perez, H.; Martínez-Castanon, G. A. The antimicrobial sensitivity of *Streptococcus mutans* to nanoparticles of silver, zinc oxide, and gold. *Nanomedicine* **2008**, *4*, 237–240.
- (54) Semmler-Behnke, M.; Kreyling, W. G.; Lipka, J.; Fertsch, S.; Wenk, A.; Takenaka, S.; Schmid, G.; Brandau, W. Biodistribution of 1.4- and 18-nm Gold Particles in Rats. *Small* **2008**, *4*, 2108–2111.
- (55) Balasubramanian, S. K.; Jittiwat, J.; Manikandan, J.; Ong, C. N.; Yu, L. E.; Ong, W. Y. Biodistribution of gold nanoparticles and gene expression changes in the liver and spleen after intravenous administration in rats. *Biomaterials* **2010**, *31*, 2034–2042.
- (56) Dikalov, S. I.; Harrison, D. G. Methods for Detection of Mitochondrial and Cellular Reactive Oxygen Species. *Antioxid. Redox Signaling* **2014**, *20*, 372–382.
- (57) Sigma Cell Proliferation Kit I (MTT) 11465007001. <http://www.sigmaaldrich.com/catalog/product/roche/11465007001?lang=en%26%AEion=CA> (accessed July, 2017).
- (58) Choi, J.; Reipa, V.; Hitchins, V. M.; Goering, P. L.; Malinauskas, R. A. Physicochemical Characterization and In Vitro Hemolysis Evaluation of Silver Nanoparticles. *Toxicol. Sci.* **2011**, *123*, 133–143.
- (59) Tomita, G. Fluorescence-Excitation Spectra of Acridine Orange-DNA and -RNA Systems. *Biophysik* **1967**, *4*, 23–29.

(60) Sayed, M.; Krishnamurthy, B.; Pal, H. Unraveling multiple binding modes of acridine orange to DNA using a multispectroscopic approach. *Phys. Chem. Chem. Phys.* **2016**, *18*, 24642–24653.

(61) Institute for Laboratory Animal Research (U.S.), & (U.S.), N.A. *Guide for the Care and Use of Laboratory Animals*, 8th ed.; National Academies Press, 2010.

(62) Parasuraman, S.; Raveendran, R.; Kesavan, R. Blood sample collection in small laboratory animals. *J. Pharmacol. Pharmacother.* **2010**, *1*, 87–93.